35th Annual International Conference of the IEEE EMBS
Osaka, Japan, 3 - 7 July, 2013

Effective Digitized Spatial Size of Unit Dipole Field in Quantitative Susceptibility Mapping*

Mai Murashima[1], Tomohiro Ueno[2], and Naozo Sugimoto[2]

***Abstract*— Quantitative Susceptibility Mapping (QSM) calculates a distribution of tissue magnetic susceptibility difference *in vivo* using measured magnetic field perturbation. The magnetic field perturbation can be approximated in first order by convolution of the susceptibility distribution with a spatial unit dipole field. Since the convolution has to be done in all space, a novel technique using harmonic properties of the dipole field is introduced to confine the calculation within the measurable region. However, discretized dipole field does not satisfy the harmonic property near its orign. Here, we investigate an effective spatial size of the dipole field in relation with the nonharmonic property using Shepp-Logan phantoms including partial volume effects. This study suggests that the dipole field can be effectively restricted to 15 voxels in diameter and that this value relates with the nonharmonic region of the discretized dipole field. Moreover, the effective size in a real space is scaled with a spatial resolution of a QSM experiment.**

I. INTRODUCTION

Magnetic susceptibility is an intrinsic physical tissue property. In order to quantify a spatial distribution of local tissue magnetic susceptibility, a novel technique of MRI called quantitative susceptibility mapping (QSM) has emerged. In MRI, local magnetic susceptibility induces nonlocal magnetic field perturbations to an applied external magnetic field. QSM has to solve nonlocal inversion problem of the magnetic field perturbations to obtain the local magnetic susceptibility. The magnetic field perturbation can be approximated in first order by a spatial convolution of the magnetic susceptibility distribution with a spatial unit dipole field. Since the Fourier transformed dipole field has zero value on two conical surfaces in *k*-space, the resulting zero division prohibits direct inversion in QSM[1]. In addition to the ill-posed nature of the inverse problem, the spatial convolution has to be done in the infinite range even though measurable magnetic field perturbations are limited in field of view (FOV) of MRI. Even in FOV, there are several regions where magnetic susceptibility is different from the surrounding tissue but a signal is not measurable in MRI, such as bone and air. Therefore, the ill-posed inverse problem has to be solved using incomplete data of the magnetic field perturbations.

*This work was supported in part by the Grants-in-Aid for Scientific Research of the Japan Society for the Promotion of Science under Grant 22700470 and Grant 20300157.

[1]M. Murashima was with the Human Health Science, Graduate School of Medicine, Kyoto University, Kyoto, Kyoto 606-8507, Japan. She is now with Toshiba Medical Systems Corporation, Otawara-shi, Tochigi-ken 324-0036, Japan.

[2]T. Ueno and N. Sugimoto are with the Human Health Science, Graduate School of Medicine, Kyoto University, Kyoto, Kyoto 606-8507, Japan (corresponding author (T.U.) to provide phone: +81-75-751-3938; fax: +81-75-751-3962; e-mail: ueno.tomohiro.2u@kyoto-u.ac.jp).

Two background field removal methods utilizing mathematical properties of the spatial unit dipole field have been proposed to confine the convolution of magnetic susceptibility to measurable regions of FOV[2], [3], [4], [5], [6]. The dipole field is a harmonic function except for its origin and satisfies Laplace's equation in the same region. The one exploits the spherical mean value property of the harmonic dipole field (SMV) to remove contributions from other than measurable regions[2], [3], [4], [5]. The other focuses on that the dipole field decays with the cube of the distance ($\sim r^{-3}$). It is formulated that the dipole field originating from measurable region is orthogonal to the one from the outside in Hilbert space of the field and that the projection theorem in Hibert space can be applied[6].

In spatially sampled dipole field, however, zero value is not derived by a digital Laplacian operator, especially near its origin. This discrepancy in the harmonic nature between the spatially sampled dipole field and the continuous one brings uncertainties to background field removal in QSM. Moreover, an effect of the dipole field on the magnetic field perturbations becomes a slow decaying function of the distance ($\sim r^{-1}$) since larger volume ($\sim 4\pi r^2 \Delta r$) has to be included into calculation at longer distance. Intuitively, this does not fit to what Liu *et al.* implicitly suggested in [6]. We have investigated the relation of the background field removal with effective size of the dipole field and have presented preliminary results at the ISMRM conference[7]. Here, we present a further investigation of spatial sampling and size effects on QSM by simulations with a Shepp-Logan digital brain phantom[8], [9] including partial volume effects.

II. THEORY

The magnetic susceptibility of human tissue, χ, is usually ~ -10ppm and can be approximated $\chi \ll 1$. When a strong external magnetic field, B_0, is applied along the z-direction, only the z-component of the induced magnetization, M_z, is dominant and can be written by $M_z = \chi B_0 \mu_0^{-1}$. μ_0 is the vacuum permeability. Therefore, we can safely omit from calculation of QSM other than the z-component of the magnetic field perturbation due to the magnetization. Then the z-component of normalized magnetic field perturbation, $\delta b_z(\mathbf{r})$, due to a magnetic susceptibility distribution, $\chi(\mathbf{r})$, is given in first order by

$$\delta b_z(\mathbf{r}) = \int_V \chi(\mathbf{r}') d_z(\mathbf{r} - \mathbf{r}') d\mathbf{r}'. \quad (1)$$

978-1-4577-0216-7/13/$26.00 ©2013 IEEE

In (1), $d_z(\mathbf{r})$ is a spatial unit dipole field and is defined by

$$d_z(\mathbf{r}) = \frac{3\cos^2\theta - 1}{4\pi r^3}, \quad (2)$$

where θ is the angle between the z-direction and $\mathbf{r}$. Since (1) includes the Lorentz sphere correction, $d_z = 0$ at $\mathbf{r} = \mathbf{0}$[1], [10]. In QSM, (1) has to be solved so as to obtain $\chi(\mathbf{r})$.

The integration volume, V, of (1) is infinite and should be limited within measurable volume, V_{in}. Since the contribution to $\delta b_z(\mathbf{r} \subseteq V_{in})$ from the outside of V_{in} (the background field) does not have any field source within V_{in}, V can be limited to V_{in} by utilizing SMV of the background field, hence of d_z. According to SMV, the mean value of spherical integration of the harmonic function equals to the value at the center of the sphere. Therefore, the contribution of the background field can be eliminated from (1) by applying an operator, $\delta - \rho$, where δ is an unit impulse function and ρ is a mean value of a spherical sum, on the both sides of (1). Since the MRI signal can not be obtained in the outside of V_{in}, $\delta - \rho$ is meaningful only in V_{in}. This means that applying $\delta - \rho$ restricts effective spatial size of d_z.

The spatially sampled dipole field has to be used in (1). As can be seen from (2), $d_z(\mathbf{r})$ changes very rapidly near its origin. It means that the partial volume effects become larger near the origin and that the voxel size is not small enough for digital differentiation. Even in the outside of the sphere of ρ, the spatially sampled dipole field originating from close to the sphere does not satisfy the SMV.

III. METHODS

A. Digital Phantoms Including Partial Volume Effects

An oversampled 3D Shepp-Logan phantom (SL1) was created at the matrix size of $(32 \times 7)^3$. The SL1 was consist of a large prolate spheroid (ps4) with an outer shell, where the major axis was 28×7 voxels long and the minor axis was 22×7 voxels long, including three smaller prolate spheroids (ps1∼3), as shown in Fig. 1 (a). Each prolate spheroid (ps$i$) was assigned its own magnetic susceptibility (χ_i) as $0.3, 0.2, 0.2$ and 0.1ppm for ps1∼4. The susceptibility values of the shell and a background were set to 1 and 0ppm, respectively. These susceptibility values were taken from [11] and tabulated in Table I, together with other phantoms' values. The susceptibility distribution of SL1 was convolved with the spatial unit dipole field, which matrix size was $(31 \times 7)^3$, to obtain the normalized magnetic field perturbation, δb_z. The expanded part was trimmed to keep central part of δb_z ($(32 \times 7)^3$) for further processing (Fig. 1 (b)). In order to simulate an MRI signal, the trimmed δb_z in the regions of the shell and the background was set to zero. Then, the oversampled δb_z was downscaled to the input matrix size, 32^3, by averaging every 7^3 voxels (Fig. 1 (c)) and used as the starting point of QSM in order to avoid complication of phase unwrapping. The resulting δb_z clearly includes partial volume effects of MRI measurements and minimizes effects from higher order terms of the dipole field approximation of magnetic field perturbations near an object boundary which is pointed out in [12]. Then a white Gaussian noises was added to have signal to noise ratios (SNR) 20. In Fig. 1 (d), a downscaled susceptibility distribution of SL1 is shown. Fig. 1 (d) corresponds to the susceptibility distribution to be obtained in QSM.

TABLE I
ASSIGNED SUSCEPTIBILITY VALUES IN SHEPP-LOGAN PHANTOMS

region \ phantom	SL1	SL2, SL3	SL4
ps1 (χ_1)	0.3ppm	0.3ppm	0.2ppm
ps2 (χ_2)	0.2ppm	0.2ppm	0.3ppm
ps3 (χ_3)	0.2ppm	0.2ppm	0.3ppm
ps4 (χ_4)	0.1ppm	0.1ppm	0.1ppm
ps5 (χ_5)	-	0.4ppm	-
shell	1ppm	1ppm	1ppm
background	0ppm	0ppm	0ppm

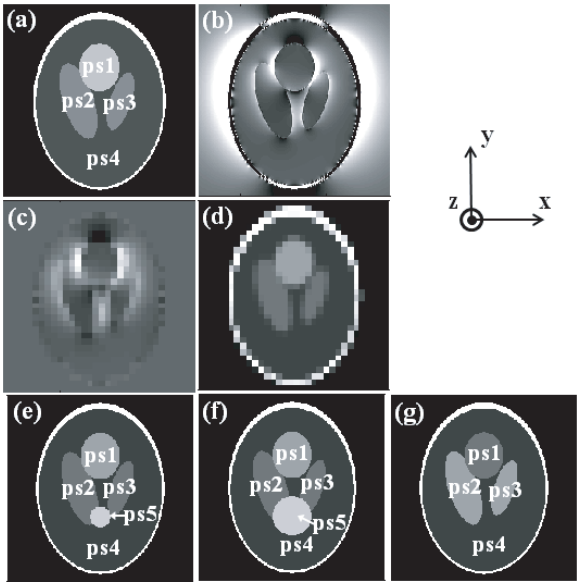

Fig. 1. Central slices of Shepp-Logan susceptibility phantoms. (a) shows an oversampled susceptibility map (matrix size: $(32 \times 7)^3$). (b) shows a normalized magnetic field perturbation map calculated from (a) (matrix size: $(32 \times 7)^3$). (c) shows a magnetic field perturbation map downscaled from trimmed (b) (matrix size: 32^3). (d) shows a susceptibility map downscaled from (a) (matrix size: 32^3). (e)-(g) show different configurations of assigned susceptibility values (matrix size: $(32 \times 7)^3$). (e) and (f) have four inner prolate spheroids and (g) has differently assigned susceptibility values.

B. Susceptibility Estimation

The operator, $\delta - \rho$, was applied on the input δb_z and removed "back ground field". As for ρ, a filled sphere of 9 voxels in diameter (D_ρ) was used. In the case of comparing size effects of ρ, four different diameters of ρ (D_ρ) was employed ($D_\rho = 5, 7, 9, 11$ voxels). ρ was consist of voxels which distance from the center (r) satisfied $(\frac{D_\rho - 1}{2})^2 \leq r^2 < (\frac{D_\rho + 1}{2})^2$. After applying $\delta - \rho$, the only region of 5 voxels

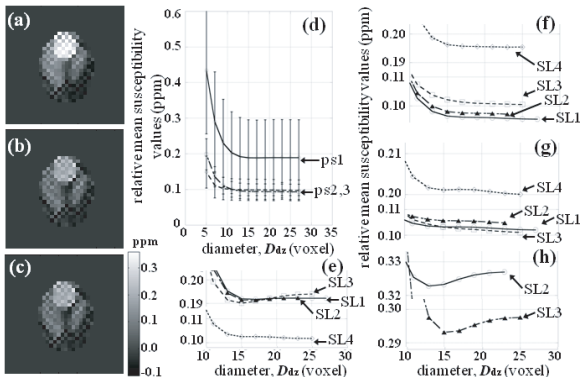

Fig. 2. Size dependence of the dipole field on susceptibility calculations. Obtained susceptibility maps of SL1 using 3 different diameters, D_{dz} =: (a) 7 voxels; (b) 15 voxels; (c) 25 voxels, are shown. (d) shows dipole field size dependence of the relative mean susceptibilities, $\Delta\chi$, of ps1-3 in SL1. Blowups of the dipole field size dependence of $\Delta\chi$: (e) of ps1 in SL1-4; (f) of ps2 in SL1-4; (g) of ps3 in SL1-4; (h) of ps5 in SL2, 3 are shown.

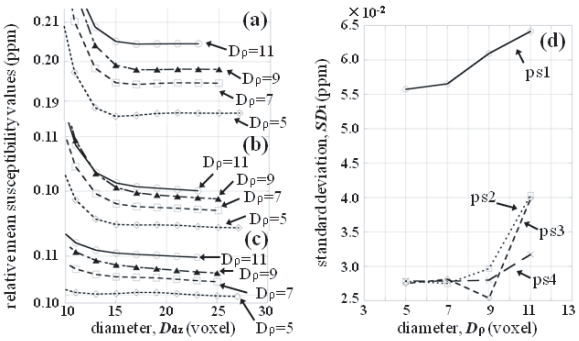

Fig. 3. Dipole field size dependence on susceptibility calculations using different sizes of the background field removal operator, $\delta - \rho$. Blowups of the dipole field size dependence: (a) of $\Delta\chi_1$; (b) of $\Delta\chi_2$; (c) of $\Delta\chi_3$ are shown. (d) shows a change of standard deviations of calculated susceptibility values, χ, with the diameter of the background field removal operator, D_ρ.

(for $D_\rho = 11$, 6 voxels) inside from the measured δb_z was extracted for later processing of QSM.

Since susceptibility anisotropy did not exist in the Shepp-Logan phantoms, the multiple orientation method[1], [13] was employed to fill missing data resulting from zero value of Fourier transformed dipole field on the two conical surfaces in *k*-space. By rotating the direction of the external magnetic field against the major axis of ps4 in three different angles (0°, 30° and 60°), three δb_z distributions were calculated. Since the convolution is a linear operation, (1) can be written as an equation of a matrix of d_z and a vector of δb_z[14]. The susceptibility distribution was estimated in the spatial domain by solving the inverse problem of three matrix-vector equations, where $\delta - \rho$ was multiplied on both sides[15]. The dipole fields with different diameters ($D_{dz} = 5 \sim 27$ voxels) and with 3 different oversampling factors ($n_{os} = 1, 3, 5$) were used. The oversampled dipole field of the n_{os} oversampling factor was created as following; each voxel was divided into n_{os}^3 isocubic subvoxels and the dipole field at each subvoxel was averaged within the voxel. For each prolate spheroid (ps$i$), mean susceptibility (χ_{mi}) and its standard deviation (SDi) were calculated only in the region corresponding to the homogeneous part of the downscaled susceptibility distribution and the relative mean susceptibilities to χ_{m4} ($\Delta\chi_{mi} = \chi_{mi} - \chi_{m4}$) were evaluated.

Calculations were done on a DELL PRECISION T3400 with a 3.00 GHz Intel(R) Core^{TM}2 Duo CPU E8400 and 16 GB memory and on a Mac Pro with a 2.66 GHz Quad Core Intel Xeon and 16 GB memory using MATLAB R2012b 64-bit. The LSQR algorithm in MATLAB was used in solving the inverse problem.

IV. RESULTS

A. Size Dependence of the Dipole Field

In Fig. 2 (a)-(c), three center slices ($z = 17$) of susceptibility maps of SL1 calculated by using three different diameters of the dipole field ($D_{dz} = 7, 15, 25$ voxels) and $D_\rho = 9$ voxels are shown. In Fig. 2 (a), the boundary between ps1 and ps2 were blurred and the image contrast was different from Fig. 1 (d), but not in Fig. 2 (b), (c). There is no significant difference between Fig. 2 (b) and (c). In Fig. 2 (d), relative mean susceptibility values, $\Delta\chi_{1-3}$, of SL1 were plotted against the diameter of the dipole field, D_{dz}. The $\Delta\chi_{1-3}$ decrease as D_{dz} becomes larger and reach constant values around $D_{dz} = 15, 17$ voxels, though $\Delta\chi_3$ shows a different dependence and an overestimated value. Above $D_{dz} = 15$ voxels, differences of calculated $\Delta\chi_{1-3}$ from assigned values are around 10^{-2}ppm and standard deviations of calculated χ_{1-4} are 6×10^{-2}ppm, 3×10^{-2}ppm, 3×10^{-2}ppm, 3×10^{-2}ppm, respectively.

In Fig. 2 (e)-(h), relative mean susceptibility values, $\Delta\chi_{1-3,5}$, of different configurations of Shepp-Logan phantoms (SL1-4) were plotted against D_{dz} only above $D_{dz} = 10$ voxels. Although slight deviation exists, $\Delta\chi_{1-3,5}$ reach constant values at $D_{dz} = 15$ voxels.

B. Size Effects of the Background Field Removal Operator

In Fig. 3 (a)-(c), the relative mean susceptibility values, $\Delta\chi_{1-3}$, in SL1 calculated with $D_\rho = 5, 7, 9, 11$ voxels were plotted against the diameter of the dipole field, D_{dz}, only above $D_{dz} = 10$ voxels. As D_ρ increases, $\Delta\chi_{1-3}$ reach constant values at a larger diameter of the dipole field, D_{dz} and the constant values increase. Fig. 3 (d) shows standard deviations of calculated susceptibility values, SD1-4, by using $D_{dz} = 15$ voxels and different D_ρ. SD1-4 shows a slight tendency to increase as D_ρ increases.

C. Effects of Oversampling Factor

Fig. 4 (a)-(c) show differences of oversampling factors, $n_{os} = 1, 3, 5$, in size dependences of three relative mean susceptibility values, $\Delta\chi_{1-3}$, in SL1 calculated with $D_\rho = 9$ voxels. $\Delta\chi_{1-3}$ with $n_{os} = 3, 5$ show almost same values and reach slightly larger constant values than that with $n_{os} = 1$ (without oversampling) does. In all n_{os}, at least 15 voxels in diameter, D_{dz}, are required to reach the constant value.

The normalized dipole fields with $n_{os} = 1, 3$ were applied by the Laplacian and the background field removal operators with different D_ρ and the resulting functions were plotted

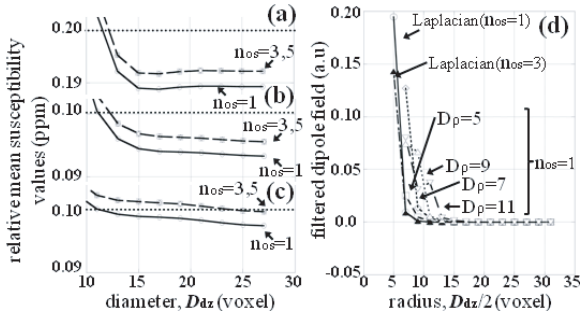

Fig. 4. Effects of the oversampling factor, n_{os}, on susceptibility calculations. The dipole field size dependence: (a) of $\Delta\chi_1$; (b) of $\Delta\chi_2$; (c) of $\Delta\chi_3$ by using $n_{os} = 1, 3, 5$ are shown. The Laplacian and the background field removal operators were applied to the normalized dipole field. (d) shows the filtered dipole field with $n_{os} = 1, 3$ along the $\theta = 0$ direction.

against the diameter of the dipole field along the $\theta = 0$ direction in Fig. 4 (d). Here, normalization was done by the maximum value of the dipole field with $n_{os} = 1$. The deviation from the harmonic property becomes larger as approaching to the origin of the field and its effects expands by applying $\delta - \rho$ with a larger diameter. However, the dipole fields with $n_{os} = 1, 3$ show almost same behavior.

V. DISCUSSIONS

This investigation suggests that the spatial size of the dipole field can be restricted to diameter of 15 voxels for estimating a susceptibility distribution. This 15 voxels diameter is smaller than the value, 21 voxels, we have presented as a preliminary result in [7]. While an sufficient value is taken accounting for slight changes of the relative mean susceptibility values, $\Delta\chi_m$, in [7], a starting point diameter is taken in this investigation since the determined diameter is rather robust in various configurations of assigned susceptibility values, such as in SL1-4, for smaller D_ρ.

As suggested in II, the diameter for restriction increases with the spatial size of $\delta - \rho$. It is always a few voxels larger than that of $\delta - \rho$. Since deviation of the digitized dipole field from the harmonic nature is remarkable within a sphere of a few voxels in radius (Fig. 4 (d)), this difference can be explained by that the outer shell having a thickness of a few voxels acts as a nonharmonic region to the $\delta - \rho$ background field removal and that the dipole field needs a few more voxels in radius for sufficient estimation of a susceptibility distribution. A larger size of $\delta - \rho$ have the larger outer shell, and it may explain larger SD1-4 in Fig. 3 (d).

Since oversampling does not improve the nonharmonic nature (Fig. 4 (d)), the relative mean susceptibility values with $n_{os} = 3, 5$ may show the same global tendency as that with $n_{os} = 1$. Slight increase of the constant value may be explained by that averaging lowers absolute values of the oversampled dipole field near the origin.

In this investigation, we ignored inhomogeneity of an external magnetic field. However, the inhomogeneity can be approximated by spherical harmonic expansions and lower orders of the expansion can be easily removed by the $\delta - \rho$ due to their slowly changing nature.

Since our numerical simulations are normalized in physical length, the determined diameter for restriction of the dipole field is not assigned to real spatial length. This means that effective length of the dipole field in real space depends on a spatial resolution of an MRI experiment. If effective physical length is needed, the resolution has to be multiplied. This can be understood from that the spatial size restriction originates mainly from digitalization of the dipole field after the background field removal and that discretization of the rapidly changing function kills digital harmonic property near the origin even in a higher resolution image.

ACKNOWLEDGMENT

We are grateful to Dr. Koji Sakai for stimulating discussions.

REFERENCES

[1] J. P. Marques and R. Bowtell, "Application of a Fourier-Based Method for Rapid Calculation of Field Inhomogeneity Due to Spatial Variation of Magnetic Susceptibility," *Concepts Magn. Reson. B (Magn. Reson. Eng.)*, vol. 25B, no. 1, pp. 65-78, 2005.

[2] L. Li and J. S. Leigh, "High-Precision Mapping of the Magnetic Field Utilizing the Harmonic Function Mean Value Property," *J. Magn. Reson.*, vol. 148, pp. 442-448, 2001.

[3] F. Schweser, A. Deistung, B. W. Lehr, and J. R. Reichenbach, "Quantitative imaging of intrinsic magnetic tissue properties using MRI signal phase: An approach to in vivo brain iron metabolism?" *Neuroimage*, vol. 54, pp. 2789-2807, 2011.

[4] C. J. G. Bakker, H. de Leeuw, and P. R. Seevinck, "Selective depiction of susceptibility transitions using Laplace-filtered phase maps" *Magn. Reson. Imag.*, vol. 30, pp. 601-609, 2012.

[5] F. Schweser, A. Deistung, K. Sommer, and J. R. Reichenbach, "Toward Online Reconstruction of Quantitative Susceptibility Maps: Superfast Dipole Inversion" *Magn. Reson. Med.*, DOI 10.1002/mrm.24405.

[6] T. Liu, I. Khalidov, L. de Rochefort, *et al.*, "A novel background field removal method for MRI using projection onto dipole fields (PDF)," *NMR Biomed.*, vol. 24, pp. 1129-1136, 2011.

[7] M. Murashima, T. Ueno, and N. Sugimoto, Comparisons of Quantitative Susceptibility Mapping (QSM) by using restricted oversampled spatial unit dipole field, in *Proc. 21st Annu. Meeting of ISMRM*, Salt Lake City, UT, 2013.

[8] L. A. Shepp and B. F. Logan, "Reconstructing Interior Head Tissue From X-Ray Transmissions," *IEEE Trans. Nuclear Science*, vol. 21, no. 1, pp. 228-236, 1974.

[9] L. A. Shepp and B. F. Logan, "The Fourier Resonstruction of a Head Section," *IEEE Trans. Nuclear Science*, vol. NS-21, pp. 21-43, June, 1974.

[10] Y.-C. N. Cheng, J. Neelavalli, and E. M. Haacke, "Limitations of Calculating Field Distributions and Magnetic Susceptibilities in MRI using a Fourier Based Method," *Phys. Med. Biol.*, vol. 54, no. 5, pp. 1169-1189, Mar, 2009.

[11] B. Wu, W. Li, A. Guidon, and C. Liu, "Whole Brain Susceptibility Mapping Using Compressed Sensing," *Magn. Reson. Med.*, vol. 67, pp. 137-147, 2012.

[12] K. M. Koch, X. Papademetris, D. Rothman, and R. A. de Graaf, "Rapid calculations of susceptibility-induced magnetostatic field perturbation for *in vivo* magnetic resonance," *Phys. Med. Biol.*, vol. 51, pp. 6381-6402, 2006.

[13] T. Liu, P. Spincemaille, L. de Rochefort, *et al.*, "Calculation of Susceptibility Through Multiple Orientation Sampling (COSMOS): A Method for Conditioning the Inverse Problem From Measured Magnetic Field Map to Susceptibility Source Image in MRI," *Magn. Reson. Med.*, vol. 61, pp. 196-204, 2009.

[14] L. Li and J. S. Leigh, "Quantifying Arbitrary Magnetic Susceptibility Distributions With MRI," *Magn. Reson. Med.*, vol. 51, pp. 1077-1082, 2004.

[15] F. Schweser, A. Deistung, B. W. Lehr, and J. R. Reichenbach, "Differentiation between diamagnetic and paramagnetic cerebral lesions based on magnetic susceptibility mapping" *Med. Phys.*, vol. 37, no. 10, pp. 5165-5178, Oct., 2010.